Is the photochemistry activity weak during haze events? —— A novel exploration on the photoinduced heterogeneous reaction of NO_2 on mineral dust

Tao Wang[1], Yangyang Liu[1], Yue Deng[1], Hanyun Cheng[1], Yang Yang[1], Yiqing Feng[1], Muhammad Ali Tahir [1], Xiaozhong Fang[1], Xu Dong[1], Kejian Li[1], Saira Ajmal[1], Aziz-Ur-Rahim Bacha[1], Iqra Nabi[1], Hongbo Fu[1], Liwu Zhang[1,2*], Jianmin Chen[1]

[1] Shanghai Key Laboratory of Atmospheric Particle Pollution and Prevention, Department of Environmental Science & Engineering, Fudan University, Shanghai, 200433, Peoples' Republic of China

[2] Shanghai Institute of Pollution Control and Ecological Security, Shanghai, 200092, Peoples' Republic of China

Abstract

Despite the increased awareness of heterogeneous reaction on mineral dust, the knowledge of how the intensity of solar irradiation influences the photochemistry activity remains a crucially important part in atmospheric research. Relevant studies have not seriously discussed the photochemistry under weak sunlight during haze, and thus ignored some underlying pollution and toxicity. Here, we investigated the heterogeneous formation of nitrate and nitrite on mineral dust under various illumination conditions by laboratory experiments and field observations. Observed by *in-situ* diffuse reflectance infrared Fourier transform spectroscopy (DRIFTS), water-solvated nitrate was the main product on TiO_2 surfaces, followed by other species varying with illumination condition. The nitrate formation rate grows rapidly from the dark to faint sunlight, while becomes insensitive to light intensity variation under strong irradiation. For example, the geometric uptake coefficient (γ_{geo}) under 30.5 mW/cm^2 (5.72×10^{-6}) has exceeded the 50 % of that under 160 mW/cm^2 (1.13×10^{-5}). Additionally, being negatively associated with nitrate (R^2=0.748, P<0.01), nitrite acts as the intermediate and decreases with increasing light intensity via oxidation pathways. Heterogeneous reaction on authentic dust (Kaolin) exhibits the similar uneven promotion effect and photoinduced negative association, which can be explained by the excess NO_2 adsorption under weak illumination while the sufficient photoinduced active species under strong irradiation based on the photo-electrochemical tests and concentration dependence experiments. Similar negative dependence appears in coarse particles collected during daytime (R^2=0.834, p<0.05), accompanied by the positive association during nighttime (R^2=0.632, P<0.05), suggesting illumination a substantial role in the atmospheric nitrogen cycling. Overall, for the nitrate formation, the conspicuous response under slight illumination offers opportunities to explain the secondary aerosol burst during haze episodes with weak irradiation. Additionally, high nitrite levels

accompanied by low nitrate concentrations may induce great health risk which was previously neglected. Further, Monte Carlo simulation coupled with sensitivity analysis may provide a new insight in the estimations of kinetics parameters for atmospheric modelling studies.

1 Introduction

Secondary nitrate aerosols, deriving mainly from various oxidation processes of nitrogen oxides, are of great importance in atmospheric chemistry **(Anenberg et al., 2017)**. These ubiquitous species is key for describing the composition and sources of particulate matters **(Huang et al., 2014; Schuttlefield et al., 2008)**. Nitrate is dominating atmospheric particulates with the increasing NO_x emissions from expanding urban traffic. It was investigated that the contributions of nitrate to the particle mass concentration increase throughout the pollution episodes **(Guo et al., 2014)**. However, current atmospheric models fail to capture the serve nitrate enhancement from the clean to haze period, and thus triggers the discussion on the heterogeneous reaction of NO_2 on primary aerosols **(Tan et al., 2016)**. Modelling studies indicated that nitrate formation is highly associated with airborne mineral dust **(Tan et al., 2016)**. Accounting for ~36% of the total primary aerosol emissions, mineral dust is one of the most abundant particle types in the troposphere **(Chen et al., 2012; Usher et al., 2003)**. During their global journey, many heterogeneous reactions take place on the particle surface, and further affect the atmospheric oxidation capacity **(Tang et al., 2017)**. This process has aroused widespread interest in East Asia because dust occupies a great share in fine particles due to the frequent occurrence of sand storms **(Zhang et al., 2015)**. Hence, the heterogeneous reaction of NO_2 on mineral dust is worthy of broader concerns.

As a complex mixture, mineral dust is composed of various metal components, such as SiO_2, Al_2O_3, Fe_2O_3, MgO, TiO_2, etc. Compared to the non-semiconducting components in mineral dust, TiO_2 has direct environmental implications for its photocatalysis **(Nanayakkara et al., 2014)**. TiO_2 is found in mineral dust at mass mixing ratios ranging from 0.1% to 10% depending on the exact location from where the particles were uplifted **(Ndour et al., 2008)**. Prior studies have indicated the photoinduced oxidation of trace gases by TiO_2 an essential role in the chemical balance of the atmosphere **(Chen et al., 2012)**. TiO_2-coated surfaces are frequently used in the vicinity of buildings or urban infrastructure **(Ballari et al., 2010; Ballari et al., 2011)**. It is suggested that these self-cleaning materials have a great chance of entering into the environment and then triggering series of atmospheric reactions **(Balajka et al., 2018; Langridge et al., 2009; Monge et al., 2010; Yang et al., 2018)**. Accordingly, TiO_2 is usually representative of the ubiquitous semiconducting components in atmospheric environment **(Kebede et al., 2013; Moon et al., 2018; Ponczek and George, 2018)**.

Earlier studies put close attention to varied factors influencing the heterogeneous process on mineral dust. Among these, moisture and temperature are widely mentioned and significant advances have been made **(Li et al., 2010; Tan et al., 2017; Tan et al., 2016; Wang et al., 2012)**. Although being treated as an important index in many atmospheric discussions, illumination has not been comprehensively investigated for its effects on the heterogeneous uptake of trace gases. Most remarkable studies concerned the photocatalytic effects under ultraviolet light while the intensity dependence under simulated solar irradiation was rarely explored **(Dupart et al., 2014; Guan et al., 2014; Li et al., 2010; Shang et al., 2010)**. Some researchers **(El Zein and Bedjanian, 2012)** noticed the uneven illumination effect on the heterogeneous reaction of NO_2 on TiO_2 particles while ignored the reaction process on authentic dust and the reaction mechanism behind the variation. Furthermore, nitrite owns an important position in atmospheric processes for its frequent appearance and great contributions to aerosol toxicity. However, there is little information available in literature about the pollution characteristics or reaction pathways of nitrite aerosols. Generally, how the illumination influences the uptake capacity and product species are questions urgently needs solving.

This work aims to provide a fresh perspective to explore the light dependence for the heterogeneous reaction on mineral dust. Monte Carlo simulation is introduced to evaluate the kinetics for nitrate formation. Size-segregated aerosol samples were collected and analysed to support relevant findings. This research is conductive to better understanding the illumination effects in atmospheric nitrogen cycling, and simultaneously providing extremely valid parameters for modelling studies.

2 Experimental

2.1 Materials

Commercial TiO_2 (Degussa, Germany), with an anatase-to-rutile ratio of 3:1 and a Brunauer-Emmett-Teller (BET) specific surface area (S_{BET}) of 55.83±0.35 $m^2 \cdot g^{-1}$ was employed as the photocatalytic mineral dust ***(Figure S1)***. Additionally, Kaolin particles from the Source Clay Minerals Repository (Purdue University, West Lafayette, IN), with a S_{BET} of 18.77±0.13 $m^2 \cdot g^{-1}$ was selected as the authentic mineral dust ***(Table S1)***. All chemicals were of analytical grade and obtained from Aladdin Chemical Reagent Co., Ltd. Ultrapure water (specific resistance ≧ 18.2 MΩ cm) produced from a deionizer (Direct-Q5-UV, MERCK, Germany) was used throughout the research process.

High-pure air (79% N_2 and 21% O_2, 99.9999% purity, Shanghai TOMOE Co., LTD, China) and 300 parts per million (ppm) NO_2 (N_2 dilution, 99.999% purity, Shanghai Qingkuan Co., LTD, China) were included in this

research. Prior to coming into the gas supply system, high-pure air went through silica gel and molecular sieve for drying and purification, respectively.

2.2 *In-situ* DRIFTS experiments

In-situ DRIFTS spectra were recorded on a FTIR spectrometer (Tracer-100, Shimadzu, Japan) equipped with a liquid-nitrogen-cooled mercury-cadmium-telluride (MCT) detector. General features of the setup are presented in ***Figure S2*** and previous reports **(Wang et al., 2018a; Wang et al., 2018b; Wang et al., 2018c)**. A xenon lamp (CEL-TCX250, Beijing Ceaulight Co., LTD, China) was used to provide simulated solar irradiation upon the particles ***(Figure S3)***.

Prior to each experiment, the particles were treated in a stream of high-pure air (200 ml·min^{-1}) for 60 min to remove the adsorbed water and impurities from the surfaces ***(Figure S4)***. Due to the overlapping bands of adsorbed water (~1640 cm^{-1}) and nitrogen compounds, the sample after pretreatment was exposed to humid high-pure air (RH≈30%, 100 ml·min^{-1}) for 20 min, after which the moisture absorption reaches saturation ***(Figure S5)***. A background spectrum was recorded after the process and then NO_2 calibration gas (5.12 ml·min^{-1}) was added into the DRIFTS chamber with a calculated mixing ratio of 15.33 ppm. Calibration gases with NO_2 mixing ratios of 9.20 and 21.45 ppm were also involved for the concentration dependence experiments. Herein, ten light intensity levels (0.0, 0.3, 5.4, 17.5, 23.8, 30.5, 54.5, 98.5, 128.1, and 160.0 mW·cm^{-2}) were referred based on the measurement by an optical power meter (CEL-NP2000, Beijing Ceaulight Co., LTD, China). Each test lasted 90 min, during which a series of spectra were recorded every 5 min with a resolution of 4 cm^{-1}.

2.3 *Ex-situ* flow reaction

Ex-situ reactions were performed on authentic particles (Kaolin) because the *in-situ* DRIFTS fails to clearly observe the surface products on some particles with weak reactivity. Herein, a home-designed quartz chamber ***(Figure S6)*** was employed as the flow reactor. In each test, 50 mg Kaolin was put into the chamber, followed by the exposure to 0.90 or 15.33 ppm NO_2 under diverse light intensities (0, 10, 40, 70, and 100 mW/cm^2). The particles after *in-situ* DRIFTS and *ex-situ* flow reactions were extracted by oscillation (5 min) with 4 ml water. The extraction solution was then passed through a 0.22 μm PTFE membrane filter for ion detection.

2.4 Ion analysis

The nitrate and nitrite ions were analysed by an ion chromatography (IC, 883 Basic, Metrohm, Switzerland), which consists of an analytical column (A5-250) and a guard column. The detection was conducted by using 3.2 mmol·L^{-1} Na_2CO_3 and 1.0 mmol·L^{-1} $NaHCO_3$ at a stable flow rate of 0.70 ml·min^{-1}. Multipoint calibrations were performed by means of standard solutions. Good linearity of the calibration curve was obtained with R^2>0.998.

2.5 Photo-electrochemical (PEC) test

To qualitatively evaluate the generation of electron-hole pairs under diverse illumination conditions, PEC tests were conducted by a electrochemical workstation (CHI-660D, Shanghai Chenhua Co., LTD, China) in a three-electrode cell with a quartz window **(Yang et al., 2017; Zheng et al., 2015)**. TiO_2 or Kaolin particles, serving as the working electrode, were deposited on a sheet of fluorine-tin-oxide glass with an effective area of $1cm^2$. A platinum wire and an Ag/AgCl electrode were employed as the counter and reference electrodes, respectively. The electrolyte was 0.5 mol/L $NaNO_3$. A xenon lamp (CEL-S500, Beijing Ceaulight Co., LTD, China) was used to provide simulated sunlight.

2.6 Uptake coefficient estimation

The reactive uptake coefficient, γ, is defined as the ratio of the reactive gas-surface collision rate ($d[NO_3^-]/dt$) to the total gas-surface collision rate (Z) **(Gustafsson et al., 2006)**. The equations are shown as follows.

$$\gamma = \frac{d[NO_3^-]/dt}{Z} \qquad Eq.(1)$$

$$Z = \frac{1}{4} \times A_S \times [NO_2] \times v_{NO_2} \qquad Eq.(2)$$

$$v_{NO_2} = \sqrt{\frac{8RT}{\pi M_{NO_2}}} \qquad Eq.(3)$$

Where A_s is the particle reactive surface area, v_{NO_2} is the mean velocity of NO_2 molecule, [NO_2] is the NO_2 concentration, R is the gas constant, T is the temperature, M_{NO_2} is molecular weight of NO_2 ***(Table S2)***. For *ex-situ* experiments, the nitrate formation rate can be translated by IC results. For the *in-situ* DRIFTS, the formation rate depends on the growth rate of nitrate peaks (*slope*) and the conversion factor (*f*), as described by ***Eq. (4)***.

$$\frac{d[NO_3^-]}{dt} = slope \times f \qquad Eq.(4)$$

The conversion factor (*f*), estimated to be $(2.09\pm0.16)\times10^{15}$ (ion · K-M $unit^{-1}$) in this study ***(Figure S7)***, is obtained from a calibration plot with the amount of NO_3^- versus the integrated areas for nitrate **(Tan et al., 2017; Tan et al., 2016)**. For the A_s, both geometric surface area (A_{geo}) and BET surface area (A_{BET}) are mentioned to evaluate the upper and lower limits of the γ-values (denoted as γ_{geo} and γ_{BET}, respectively) varying with reaction probabilities between reactants and particles.

Monte Carlo simulation was implemented to quantify the uncertainty and its impact on the kinetics assessment **(Chiang et al., 2009; Ginsberg and Belleggia, 2017; Xia et al., 2013)**. Each independent variable was determined via five or more replication measurements and assumed to be normally distributed in the

simulation. We performed independent runs at 1500, 3000, 5000, and 10000 iterations with each parameter. The results showed that 5000 iterations are sufficient to ensure the stability of the results. Additionally, sensitivity analysis is helpful in exploring the variables that influence the estimation most. Pearson correlation coefficients between each variable and the output (γ-value) were calculated and then normalized to 100%. On this basis, the contribution of each input variable to the output can be assessed. Three input variables are included for γ_{geo}: *slope*, *f*, and A_s. For γ_{BET}, the A_s is further divided into mass and S_{BET} as discussed above.

2.7 Particle sampling and chemical analysis

Aerosols were collected in the late summer and early autumn in the campus of Fudan University, Shanghai, China ***(Figure S9)***. The first stage from 23th August to 17th September contains 26 daily samples. The second stage lasted from 21th to 29th September, including eight sample sets collected during daytime and another eight during nighttime.

The size-segregated samples ranging from 0.4 to 100 μm were collected on quartz fiber filters (Whatman, UK) using an eight stage micro-orifice uniform deposit impactor (Anderson, Tisch Environmental Inc, USA) operating at a flow rate of 28.3 L/min. The particle modes were defined as follows: 0-0.56 μm for condensation mode, 0.56-1.8 μm for droplet mode, and 1.8-100 μm for coarse mode.

Before sampling, the filters were pre-combusted at 550℃ for 4 h to minimize original impurities. After collection, the filters were extracted ultrasonically by 20 ml water for 45 min. Water extracts were passed through a 0.22 μm PTFE membrane filter for NO_3^- and NO_2^- detection as introduced in **section 2.4**.

3 Results and discussion

3.1 Observed species on particles

Figure 1 presents the product analysis for dark reaction **(Figure 1a-c)** and illumination process **(Figure 1d-f)** by means of DRIFTS spectra, along with the quantitative evaluation of nitrate and nitrite formation based on IC measurements **(Figure 1g-i)**. Gaussian curve-fitting procedure was employed to deconvolute the overlapping bands. The fitting was undertaken until reproducible results were obtained with the coefficient of determination (R^2) greater than 0.990. The bands in the spectra are quite rich, indicating various products as summarized in ***Table S5***.

Under illumination, the signals peaking at 1312 and 1553 cm^{-1} reflect the formation of monodentate nitrate, whereas those at 1276, 1573, and 1602 cm^{-1} account for the vibration of bidentate nitrate **(Figure 1d, e) (Li et al., 2010; Ma et al., 2011; Niu et al., 2017; Szanyi et al., 2007)**. Bridging bidentate nitrate can be recognized by the shoulder peak at 1602 cm^{-1} **(Du et al., 2019; Goodman et al., 1998; Sun et al., 2016; Szanyi et al., 2005; Yi et**

al., 2007). Besides, the peaks at 1347 and 1412 cm^{-1} are assigned to water-solvated nitrate **(Baltrusaitis et al., 2007; Guan et al., 2014; Miller and Grassian, 1998)**. Under dark condition, except the similar bands appearing under illumination (1561, 1409, 1323, and 1271 cm^{-1}), some nitrite products become more attractive as evident by the monodentate nitrite at 1195 and 1440 cm^{-1}, as well as the bidentate nitrite around 1308 cm^{-1} **(Figure 1a, b) (Wu et al., 2013)**. Water-solvated nitrate is far ahead in amount compared to other species **(Figure 1c, f)**, suggesting weak links between the products and particle surfaces. Hence, the surface water layers of the hygroscopic particles provides plenty active space for the heterogeneous uptake of NO_2.

After the reversible adsorption of NO_2 on mineral dust ***(R.S1)***, the NO_2 reacts with hydroxyl-related groups (OH^-) or surface H_2O to form adsorbed nitrate/nitrite or free nitric acid/nitrous acid, respectively ***(R.S2-S3)***. Since no acid molecules were observed, free nitrite and nitrate ions stem from ionization ***(R.S4-S5)***. The disproportionation process ***(R.1)*** dominates the dark reaction. When excited with light (wavelength≤390 nm), there is the generation of electron-hole pairs in the conduction and valence bands of TiO_2 ***(R.S6)*** **(Dupart et al., 2014; FUJISHIMA and HONDA, 1972; Yu and Jang, 2018)**. Photogenerated holes and electrons react with H_2O and O_2, and thus lead to the formation of hydroxyl radicals ($^{\cdot}OH$) and reactive oxygen radicals ($O_2^{\cdot-}$), respectively ***(R.S7-S8)*** **(Chen et al., 2012)**. Superoxide hydrogen radical ($HO_2^{\cdot}$) and hydrogen peroxide (H_2O_2) appear and produce $OH^{\cdot}$ as well ***(R.S7-S14)***. These photoinduced active species (PAS) would accelerate the nitrate formation ***(R.2)***.

$$NO_2 \xrightarrow{OH^-/H_2O} NO_3^- + NO_2^- \qquad R.(1)$$

$$NO_2 \xrightarrow{h\nu \ \& \ TiO_2} NO_3^- \qquad R.(2)$$

Noticeably, nitrite (especially monodentate type) decreases in proportion as the dark reaction proceeds, together with the increasing contribution from bidentate nitrate species and water-solvated ones ***(Figure 1c, Figure S11a)***. The nitrite would react with another surface nitrite in a Langmuir-Hinshelwood mechanism ***(R.3)*** or gaseous NO_2 in an Eley-Rideal mechanism ***(R.4)*** to form nitrate in the absence of illumination **(Tang et al., 2018; Underwood et al., 1999)**. Oxygen also acts as a promoter in the nitrite oxidation **(Tang et al., 2018)**. On the other hand, diverse nitrate species make steady contributions to the total products during the photoreactions ***(Figure S11b)***. Generally, nitrite signal is visible in dark, while gradually fades away after irradiation due to the oxidation of nitrite to nitrate by PAS via ***R.5 (Section S9)***. The reactions ***R1***, ***R2***, and ***R5*** are presented in a brief way, followed by detailed processes listed in ***Section S8***.

$$2NO_2^- \rightarrow NO_3^- + NO + e^- \qquad R.(3)$$

$$NO_2^- + NO_2 \rightarrow NO_3^- + NO \qquad R.(4)$$

$$NO_2^- \xrightarrow{hv \ \& \ TiO_2} NO_3^- \qquad R.(5)$$

Different with previous studies, the dimer of NO_2, namely N_2O_4, was not observed in these spectra around 1745 and 1295 cm^{-1}. It has been confirmed that N_2O_4 could isomerize and autoionize to $NO^+NO_3^-$, and then react with adsorbed water to generate HNO_3 and HONO **(Syomin and Finlayson-Pitts, 2003)**. Meanwhile, N_2O_4 may exist in the initial stage of the whole reaction and be consumed immediately along with the oxidation of nitrite species. Liu et al., investigated the consumption of N_2O_4 during the oxidation of adsorbed SO_2 **(Liu et al., 2012)**. Herein, the proposed process can be described by ***(R.6-7)***.

$$2NO_2 \leftrightarrow N_2O_4 \leftrightarrow ONONO_2 \leftrightarrow NO^+NO_3^- \overset{H_2O}{\longleftrightarrow} HNO_3 + HONO \qquad R.(6)$$

$$NO^+NO_3^- + NO_2^- \rightarrow NO_3^- + NO^+NO_2^- \qquad R.(7)$$

Illumination has impacts on either product species or the production. The final DRIFTS spectra grow in intensity as the illumination becomes stronger. Raman measurements also indicate the drastic enhancement caused by sunlight, evident by the higher nitrate peak after illumination compared to that after dark process ***(Section S10)*** **(Fu et al., 2017; Yu et al., 2018; Zhao et al., 2018)**. These observations provide a solid evidence that the nitrate formation on mineral dust is enhanced under sunlight, in nice agreement with previous results **(Dupart et al., 2014; Guan et al., 2014)**. Noticeably, the nitrate determined by IC exhibits a clear nonlinear uptrend with increasing light intensity, suggesting uneven illumination effect on nitrate formation **(Figure 1g)**. On the contrary, the nitrite presents a nonlinear downtrend **(Figure 1h)**, and thus results in the negative association with nitrate **(Figure 1i)**.

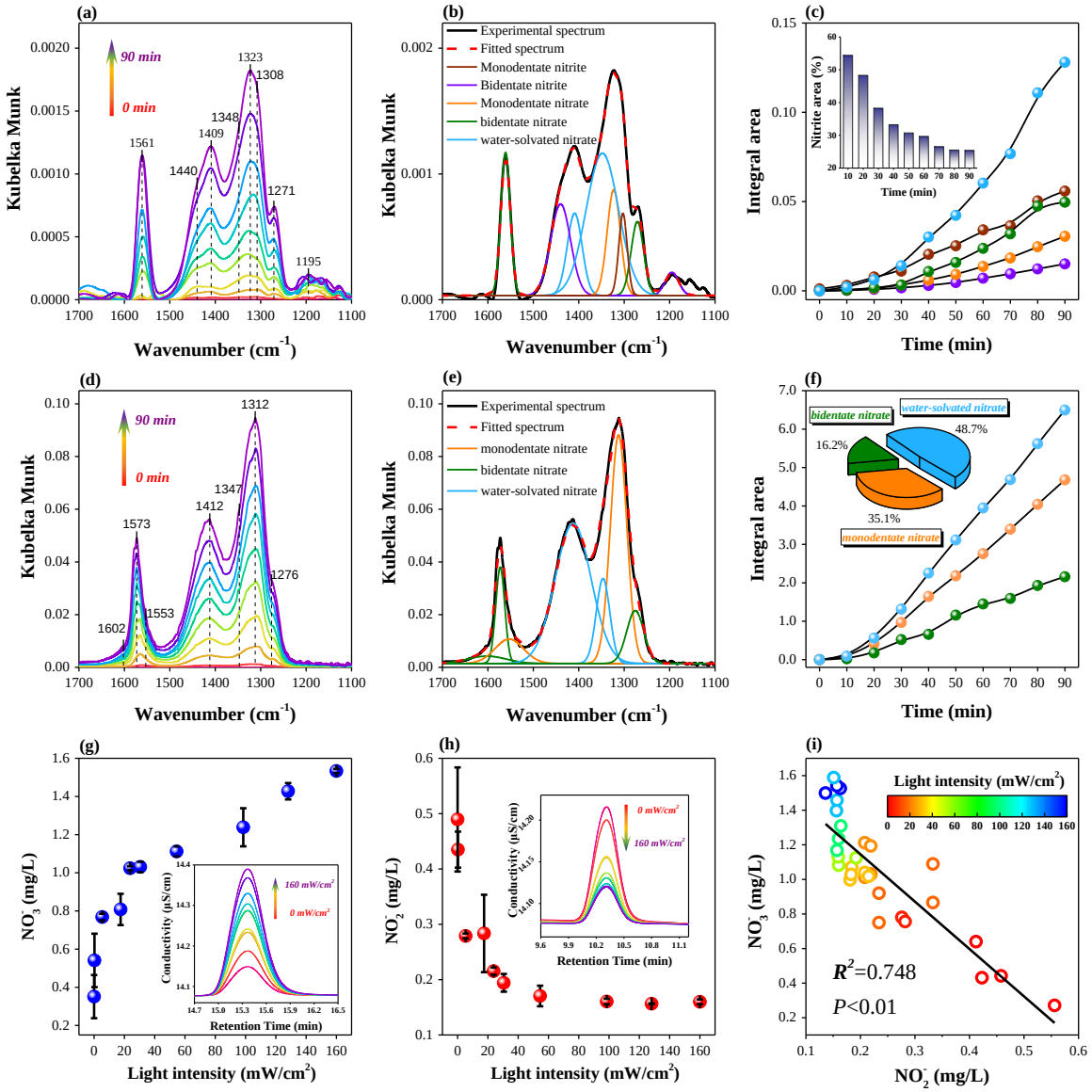

Figure 1. Product observations under **(a-c)** dark condition and **(d-f)** illumination (I=98.5 mW/cm^2), as well as **(g-i)** ion analysis results. **(a, d)** DRIFTS spectra of nitrate and nitrate species. **(b, e)** Peak fitting for the final spectra based on Gaussian method. **(c, f)** Integral areas of diverse species as a function of reaction time. IC measurements for **(g)** nitrate and **(h)** nitrite ions after DRIFTS tests. Error bars represent 1σ. **(i)** Linear association between nitrate and nitrite varying with light intensity. Inset: **(c)** Time-dependent contributions of nitrite, **(f)** Contributions of diverse products after 90 min exposure. **(g, h)** Conductivity spectra from IC.

3.2 Photoinduced uptake capacity

To accurately evaluate the photoinduced nitrate formation, γ-values were estimated based on Monte Carlo simulation with the cumulative probability distributions depicted in **Figure 2** and the percentile values summarized in ***Table S3***. γ_{BET} and γ_{geo} exhibit similar variation trends. Since the reaction is first order with respect

to NO_2 concentration under various light intensities ***(Figure S8)***, the γ-values would still be authentic for atmospheric reactions with lower NO_2 concentrations. The growth of γ-values appears to be slow after the initial fast with increasing light intensity. For instance, the γ_{geo} under 30.5 mW/cm^2 exceeds the half of that under 160 mW/cm^2. To facilitate comparison, theoretical γ-values were calculated in a linear way based on the results under 0 and 160 mW·cm^{-2}. The actual γ-values under 5.4, 17.5, 23.8, 30.5, 54.5, 98.5, and 128.1 mW·cm^{-2} are 73%, 135%, 189%, 158%, 148%, 103%, 39%, and 16% higher than the corresponding theoretical ones, respectively. This 'fast-slow' uptrend seems to be of great importance as it shows that the γ-values measured at designed irradiation intensity may not be extrapolated in a linear way to those relevant to the atmosphere.

To distinguish the contributions of each variable to the output, sensitivity analysis is performed on the basis of the simulated data. Slope and *f* contribute most to the total variance of γ_{BET} and γ_{geo}, while S_{BET} and m for γ_{BET}, and A_{geo} for γ_{geo} contribute little ***(Section S11)***. Accordingly, slope and *f* values in a more accurate level are beneficial for γ-value estimation. More attention in the future needs to be devoted to the stability of DRIFTS and IC measurements.

In view of the great significance of γ_{geo} in atmospheric models, regression analysis is employed to fit the obtained results and further predict values for relevant reactions. Since the γ-values exhibit a 'fast-slow' uptrend, a polynomial regression model ***(Eq.5)*** is used to describe the variation.

$$\gamma_{f,geo} = aI^3 + bI^2 + cI + d \qquad Eq.(5)$$

Where $\gamma_{f,geo}$ is the fitted γ_{geo}, I is light intensity, and a, b, c and d are essential parameters. The final formula ***(Eq.6)*** could explain 99.8% variation of the experimental γ_{geo}, indicating accurate regression **(Figure 2c)**. Based on this, the $d\gamma_{geo}/dI$ values are obtained by derivation to distinguish the illumination effect varying with light intensity. The uptake capacity is extremely sensitive to intensity variation under weak illumination, while tends to be insensitive under strong irradiation **(Figure 2d)**. In Shanghai (31°11'E, 121°29'W), the 3h-average solar irradiation intensities are mostly lower than 80 mW/cm^2 (NOAA data, https://www.arl.noaa.gov/), indicating noticeable sunlight impacts. More importantly, the irradiation tends to be weaker in winter **(Figure 2d)**, highlighting the central role of light-dependent heterogeneous reaction in haze events during cold time.

$$\gamma_{f,geo} = 5.62 \times 10^{-12} \times I^3 - 1.92 \times 10^{-9} \times I^2 + 2.32 \times 10^{-7} \times I + 2.93 \times 10^{-7} \qquad Eq.(6)$$

$$d\gamma_{geo}/dI = 1.686 \times 10^{-11} \times I^2 - 3.84 \times 10^{-9} \times I + 2.32 \times 10^{-7} \qquad Eq.(7)$$

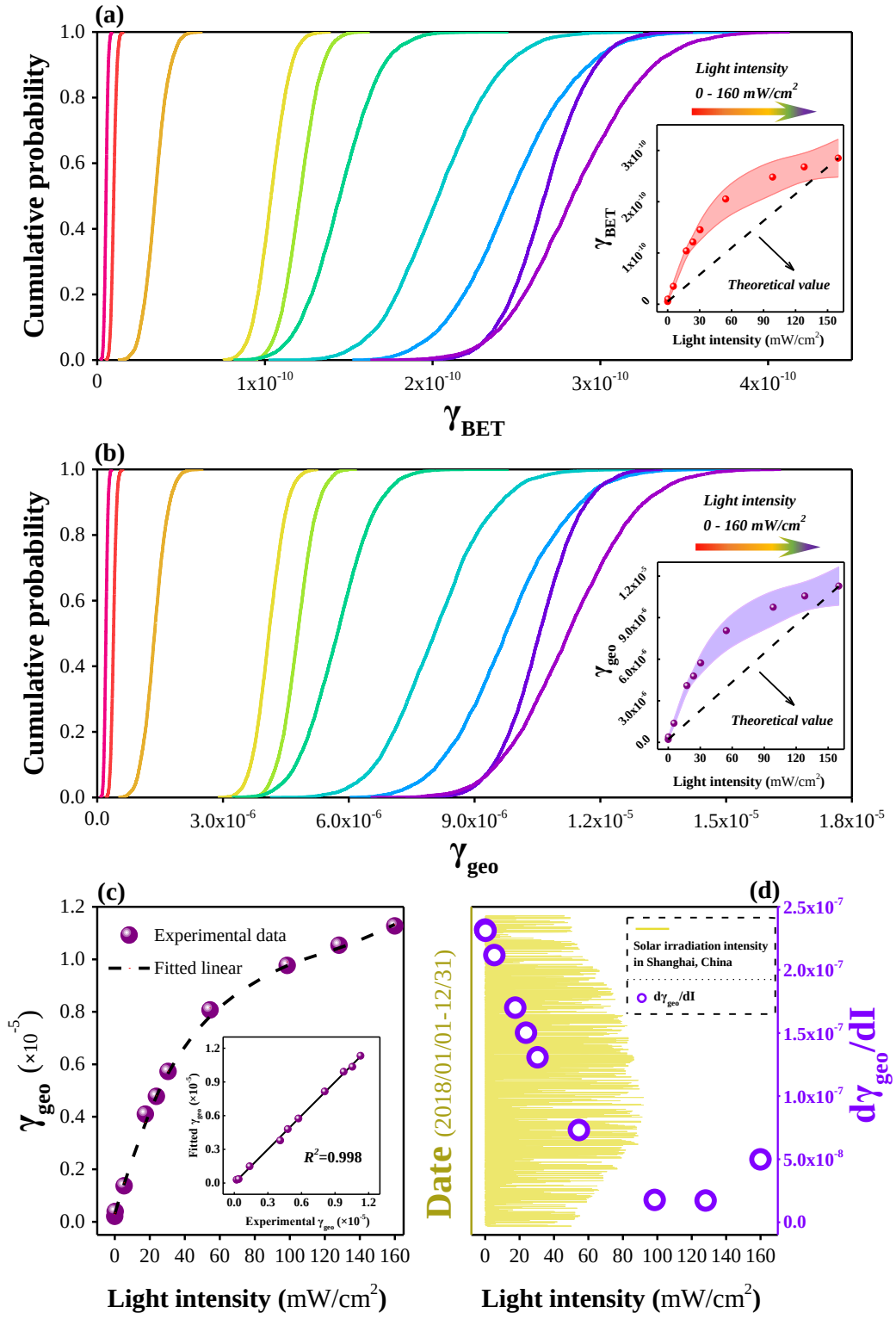

Figure 2. Cumulative probability distribution of the **(a)** γ_{BET} and **(b)** γ_{geo} values based on Monte Carlo simulation. Insets reveal the actual γ-values (Mean±1σ) and theoretical ones. **(c)** Regression analysis on γ_{geo}. Inset presents the linear relation between calculated and fitted values. **(d)** Downward short wave radiation flux (DSWF) in Shanghai, China coupled with estimated $d\gamma_{geo}/dI$.

3.3 Reaction on authentic dust

The above sections include the product observation on TiO_2 particles and the relevant kinetics evaluation. Although being ubiquitous in natural environment, TiO_2 is in representative of single-component mineral dust. Kaolin, comprising SiO_2, Al_2O_3, Fe_2O_3, TiO_2 and other components, is a more typical authentic mineral dust.

The Kaolin particles in the *ex-situ* flow reactor was exposed to NO_2 with a low mixing ratio (0.9 ppm) under diverse light intensities. Nitrate formation can be observed with increasing reaction time **(Figure 3a)**. The uptake coefficients were evaluated by Monte Carlo simulation **(Figure 3b)**, and the similar 'slow-fast' uptrend occurred again **(Figure 3c)**. The actual γ-values under 10, 30 and 70 $mW \cdot cm^{-2}$ are 246 %, 90 % and 35 % higher than the corresponding theoretical values, respectively, indicating that the uneven illumination effect on nitrate formation really exists in the atmosphere. Percentile γ-values for the heterogeneous uptake of NO_2 on Kaolin particles are summarized in ***Table S4***. Based on regression analysis (R^2=0.994), the $d\gamma_{geo}/dI$ values were estimated by derivation to distinguish the promotion effect influenced by light intensity. The nitrate formation rate on Kaolin particles appears to be sensitive to the intensity variation under faint sunlight, while tends to be insensitive as the illumination becomes stronger **(Figure 3c)**, in consistent with the situation for TiO_2. Furthermore, the negative correlation between nitrite and nitrate can be observed as well **(Figure 3d)**, suggesting the significant oxidation of nitrite under strong irradiation. The balance between PAS formation and NO_2 adsorption on mineral dust is responsible for these illumination effects, which will be carefully discussed in the mechanism section.

Noticeably, the γ_{geo} values for Kaolin are approximately two orders of magnitude lower than those for TiO_2, suggesting the weaker reactivity of authentic dust because of the low proportion of photocatalytic components. Since *in-situ* DRIFTS fails to observe the product formation on Kaolin, this quartz reactor provides a better solution to evaluating the kinetics for some authentic dust due to its greater reaction area. The measured uptake capacity under dark condition is comparable with the previous result obtained by flow tube reactor **(Liu et al., 2015)**, indicating the reliability of this new-style reactor in atmospheric laboratory research. Generally, two questions become more interesting when discussing the heterogeneous process on mineral surrogates or authentic dust: What is the association between nitrate and nitrite in atmospheric particulates? What is the proposed mechanism behind these illumination effects? We may discuss these issues in the following sections.

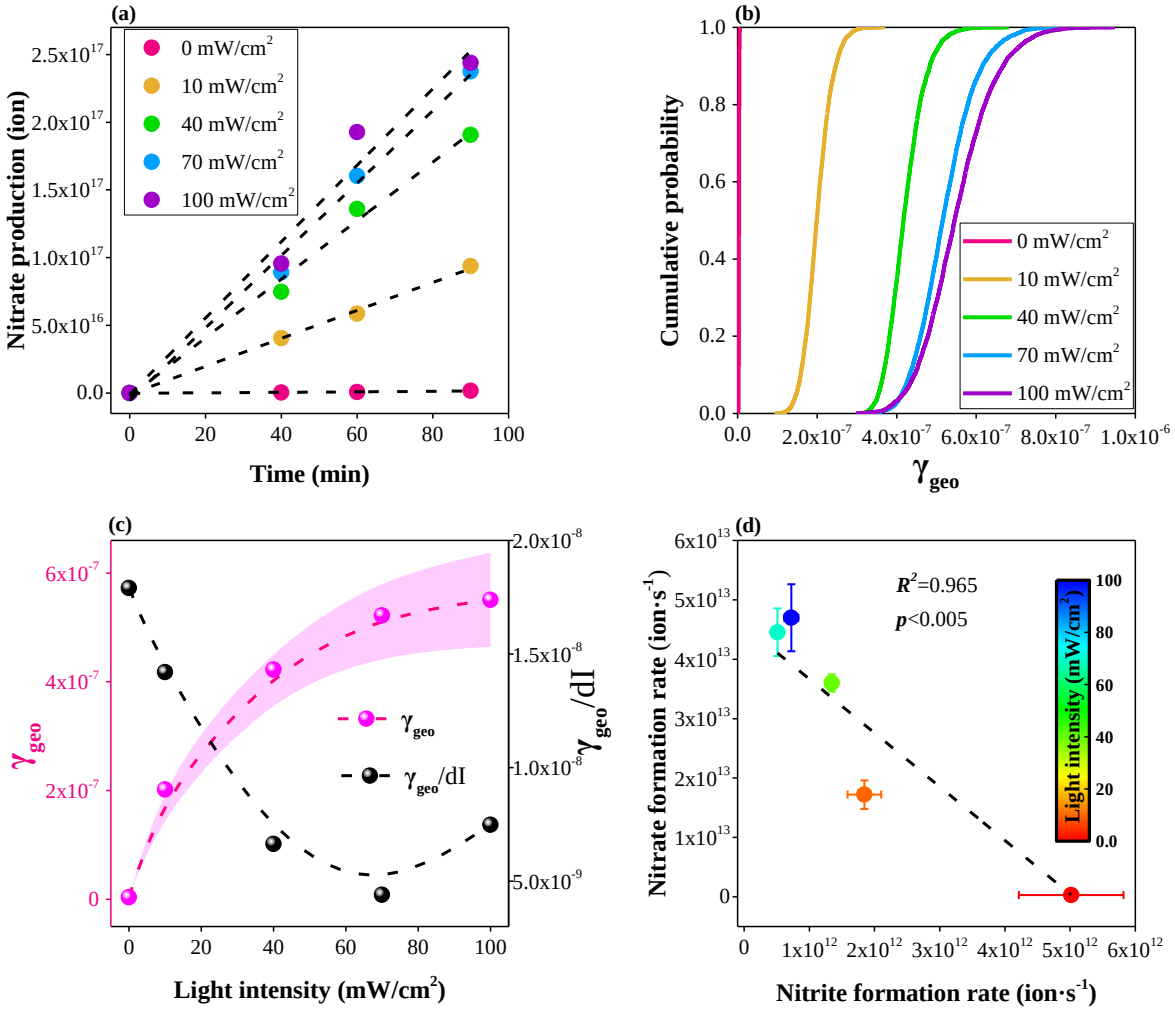

Figure 3. (a) Nitrate formation on Kaolin as a function of reaction time varying with irradiation intensity. **(b)** Cumulative probability distribution of the γ_{geo} values based on Monte Carlo simulation. **(c)** Actual γ-values (Mean±1σ) coupled with estimated $d\gamma_{geo}/dI$. **(d)** Linear association between the formation rates of nitrite and nitrate on Kaolin particles varying with light intensity.

3.4 Nitrogen redox

Figure 4 presents the association between atmospheric nitrate and nitrite varying with particle mode and sampling period. For better comparison, 26 daily samples were classified into several groups according to the nitrite concentrations. Significant positive correlation can be found during nighttime in coarse mode **(Figure 4a)**. In contrast, there is no case indicating high nitrite and nitrate levels during daytime, and the dependence seems to be negative **(Figure 4b)**. The correlation turns to be significant with the ignorance of cases where the nitrite and nitrate concentrations are extremely low. As discussed above, the associations during nighttime and daytime can be explained by the NO_2 disproportionation in the absence of sunlight and the nitrite oxidation under illumination,

respectively. Daily nitrite and nitrate concentrations exhibit the similar variation with that during daytime, and a negative correlation can be found based on the classification of nitrite levels **(Figure 4c)**.

Nitrate and nitrite from diverse periods exhibit analogous size distribution: greatest in coarse mode, followed by droplet mode and condensation mode ***(Figure S10)***. Yet, except the large mass fraction in coarse mode, nitrite presents extra peak under 1.8 μm, indicating reaction pathways differing from nitrate formation **(Moore et al., 2004)**. That is, nitrate is difficult to accumulate by aqueous reactions or homogeneous processes while nitrite seems to be easy, which results in the lower correlation coefficients for small size particles **(Figure 3d-i)**. Since the main reaction pathways on particle surfaces still take place in aqueous media, and some other oxidants (e.g. H_2O_2, O_3, and Fe^{3+}) would replace the semiconductor components in mineral dust under illumination **(Hems et al., 2017; Hou et al., 2017; Xue et al., 2016)**, the correlation in droplet mode appears to be obvious with merely lower R^2. Furthermore, both ions exhibit great mass fractions (>50%) in coarse mode, making the associations for full-size particles similar with those for coarse aerosols **(Figure 3j-l)**.

It is universally acknowledged that atmospheric nitrate may undergo photolysis ***(R.8-10)*** under acidic conditions **(Goldstein and Rabani, 2007; Schuttlefield et al., 2008; Ye et al., 2016)**. These two processes (photolysis of nitrate and oxidation of nitrite) may contribute to the negative association in different aspects. Yet, the nitrite oxidation seems to be more easily to take place because some semiconductor in the atmosphere can be excited by visible light, while the nitrate photolysis mainly occurs under ultraviolet light **(Benedict et al., 2017; Ye et al., 2017)**. The exact contributions of these two processes to this negative correlation are still not very clear. Noticeably, some aerosol samples indicate low nitrite levels accompanied by slight nitrate pollution in the presence of sunlight. Besides the photolysis of nitrate and nitrite, HONO formation in acidic media ***(R.11)*** is another sink of surface nitrous acid **(Liu et al., 2015; Su et al., 2011; Wang et al., 2015; Zhang et al., 2012)**.

$$NO_3^- \overset{h\nu}{\Rightarrow} NO_2^- + O(^3P) \qquad R.(8)$$

$$NO_3^- + H^+ \overset{h\nu}{\Rightarrow} NO_2 + {}^{\cdot}OH \qquad R.(9)$$

$$NO_3^- \overset{h\nu}{\Rightarrow} ONOO^- \qquad R.(10)$$

$$NO_2^- + H^+ \leftrightharpoons HNO_2 \leftrightharpoons HONO \qquad R.(11)$$

Generally, atmospheric nitrite is positively correlated with nitrate in the absence of irradiation, whereas presents negative association with nitrate during daytime. The dependence is significant for coarse particles while turns to be inconspicuous in droplet mode and condensation mode.

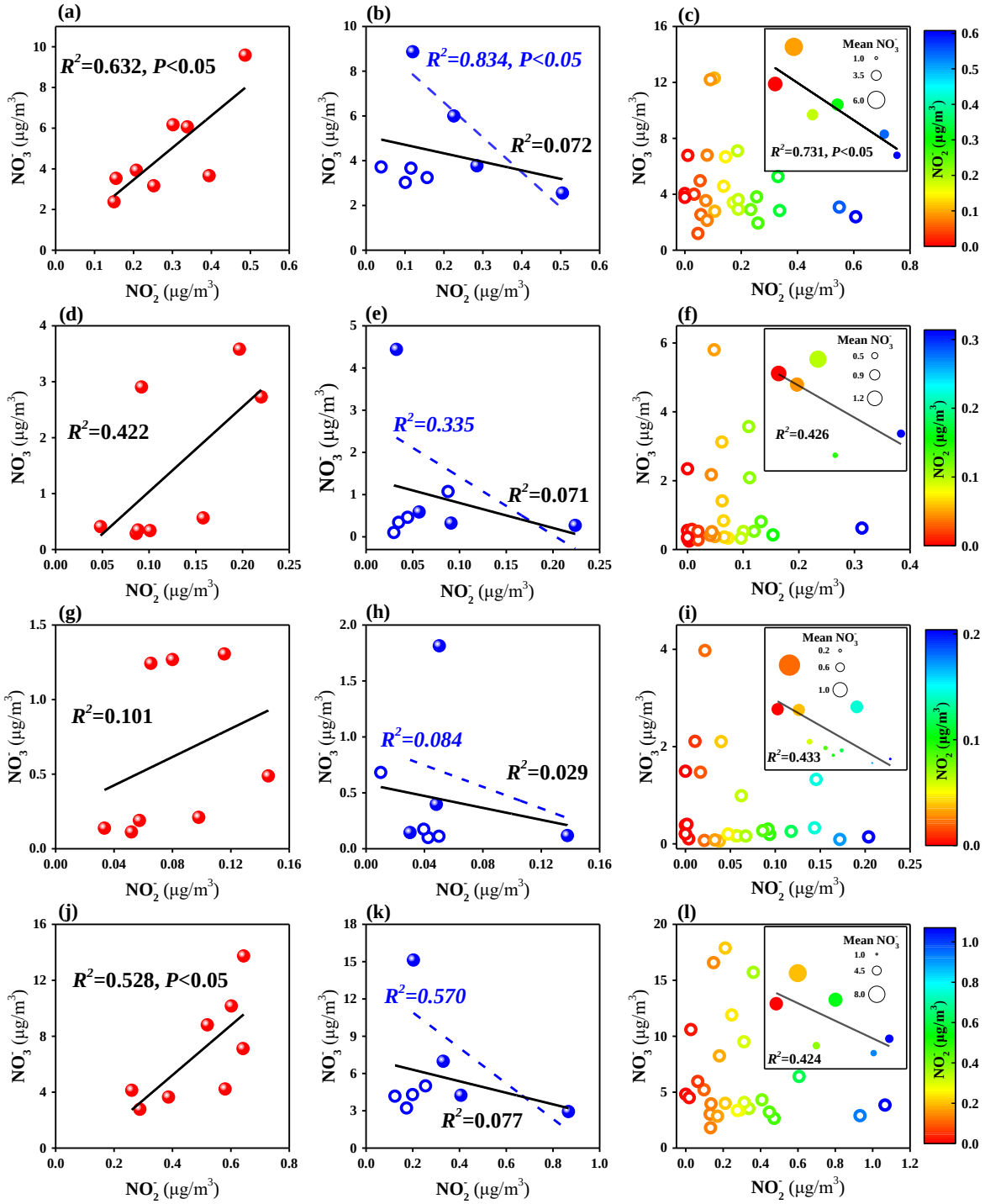

335

336 **Figure 4**. Associations between atmospheric nitrite and nitrate ions in **(a-c)** coarse mode (1.8-100 μm), **(d-f)**

337 droplet mode (0.56-1.8 μm), **(g-i)** condensation mode (0-0.56 μm), and **(j-l)** full-size particles (0-100 μm)

338 collected during **(a, d, g, j)** nighttime, **(b, e, h, k)** daytime, and **(c, f, i, l)** whole day. Insets: mean nitrate

339 concentrations based on nitrite classification. Linear correlation analysis (solid line) was employed for each case.

340 The dashed lines for daytime cases reveal the correlation for solid circles with hollow circles ignored.

3.5 Proposed mechanism

Detailed reaction pathways concerning the heterogeneous reaction of NO_2 on mineral dust have been included in previous sections. However, the uneven illumination effect cannot be explained by chemical equations. The photocurrents of both TiO_2 **(Figure 5a)** and Kaolin **(Figure 5b)** are linearly correlated with light intensity, indicating even illumination effect on the generation of electron-hole pairs. Hence, photocatalytic activity of the mineral dust is not sufficient to explain the uneven nitrate/nitrite formation with illumination variation.

Since no saturation effects were observed in each *in-situ* experiment, the NO_2 adsorption rate can be regarded as constant. Adsorbed NO_2 becomes excess compared to the formed PAS under weak sunlight, and thus makes illumination the rate-limiting factor in oxidation. At this time, nearly all the PAS participate in the oxidation of surface adsorbed NO_2 as well as some nitrite intermediates. When the illumination is strong, the PAS gradually become excess compared to the adsorbed NO_2. Under the circumstances, light makes little contribution to the elevation of uptake capacity and simultaneously NO_2 adsorption turns into the new rate-limiting factor. Generally, the balance between NO_2 adsorption and PAS formation results in the nonlinear uptrend of γ-values with increasing light intensity.

Concentration dependence was considered in this research, and the nitrate formation rates at given conditions were normalized by the corresponding result estimated at the highest light intensity. For TiO_2 **(Figure 5c)**, at low mixing ratio (9.20 ppm), the formation rate is light-dependent under weak illumination while tends to be steady with increasing light intensity, suggesting excess PAS under strong irradiation. The difference is that, at high mixing ratio (21.45 ppm) the formation rate under strong irradiation was not nearly equal to that under 160 mW/cm^2, implying sufficient adsorbed NO_2 at relatively high intensity. The trends for Kaolin are similar with those for TiO_2 particles **(Figure 5d)**. For the exposure under 0.9 ppm, the 'fast-slow' uptrend appears because of the sufficient NO_2 adsorption under weak illumination and the enough PAS under strong illumination. However, when it turns to high mixing ratio (15.33 ppm) of NO_2, the nitrate formation rate is linearly correlated with light intensity, indicating sufficient NO_2 adsorption among the simulated solar range.

In general, it could be deduced that lower NO_2 concentration makes the nitrate formation rate close to the highest level under weaker solar irradiation. On the other hand, higher NO_2 concentrations trigger broader influence scope of illumination. Hence, current serious NO_2 pollution may increase the participation of solar irradiation in the formation of secondary aerosols.

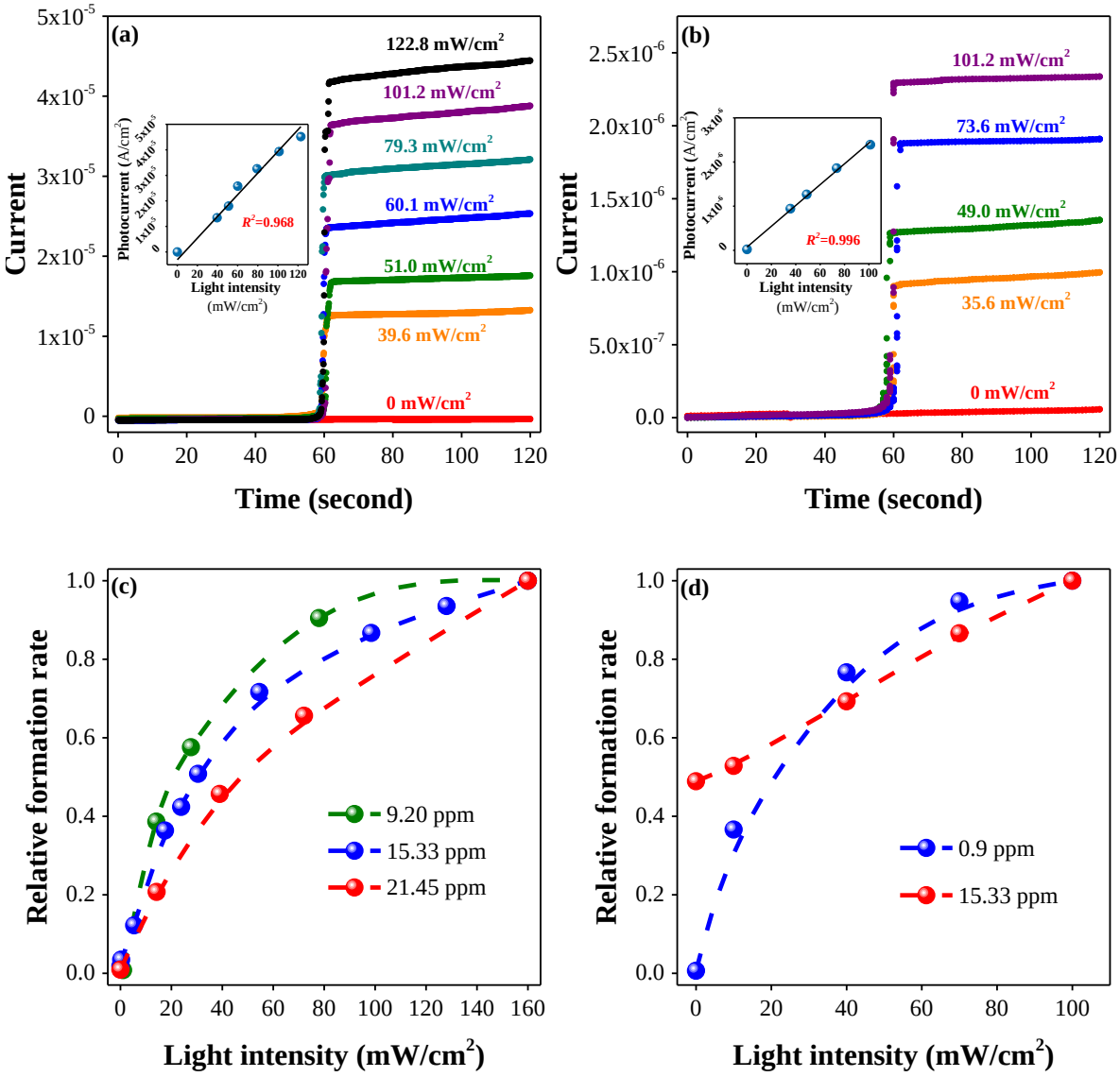

Figure 5. Current densities of **(a)** TiO_2 and **(b)** Kaolin under various light intensities (60-120 s). Inset: linear correlation between averaged photocurrent densities and irradiation intensities. Relative nitrate formation rate as a function of light intensity under different NO_2 mixing ratios for **(c)** TiO_2 and **(d)** Kaolin particles.

The balance between NO_2 adsorption and PAS formation influenced by light intensity can also be used to explain the negative association between nitrate and nitrite. Limited PAS participate in the oxidation of excess NO_2 under weak illumination, and thus make space for the nitrite formation via disproportionation process. Under strong irradiation, there are still sufficient PAS involved in the nitrite oxidation after the photochemical conversion of limited NO_2. For the oxidation of nitrite intermediates, the main promoters are NO_2 and other nitrite species under dark condition or weak illumination, while turns to be PAS under stronger irradiation. Hence, nitrite unevenly decreases with increasing light intensity, and exhibits a negative association with nitrate.

As shown in **Scheme 1**, the nitrate formation on mineral dust is light-dependent under weak illumination while NO_2-dependent under strong illumination. Light triggers atmospheric reactions with different features, and simultaneously results in diverse proportions of nitrogen species. Nitrite-rich and nitrate-rich products may occupy the mainstream under faint sunlight and strong irradiation, respectively.

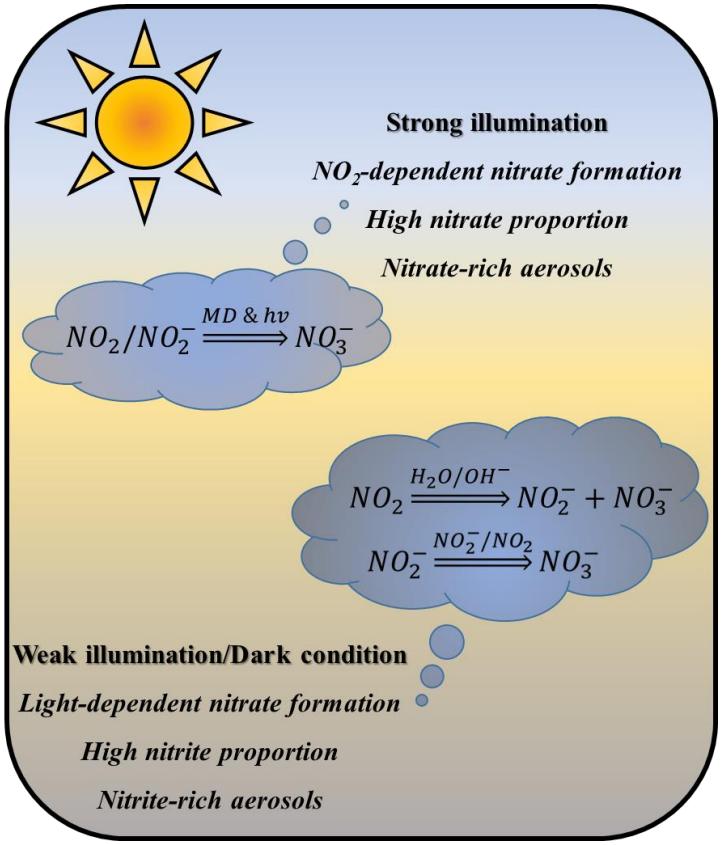

Scheme 1. Characteristics of the photoinduced heterogeneous reaction of NO_2 on mineral dust (MD) under different illumination conditions.

4 Conclusions

The heterogeneous reaction of NO_2 on TiO_2 and Kaolin particles was investigated by means of *in-situ* DRIFTS experiments and *ex-situ* flow reactions, respectively. Photochemistry has traditionally been considered inapparent during haze events due to the weak sunlight near the ground caused by low visibility. Hence, light intensity is taken into consideration as an important index. For better illustration, size-segregated aerosol samples were collected in the absence and presence of sunlight.

Water-solvated nitrate is the main product on TiO_2 surfaces, followed by other species influenced by illumination conditions. The nitrate formation rate is enhanced by simulated solar irradiation with uneven promotion effect. The nitrate formation is sensitive to the variation of light intensity under weak illumination, while tends to be insensitive under strong irradiation. That is, the uptake coefficient for NO_2 adsorption under

moderate sunlight is close to that under strong irradiation. The oxidation of nitrite can be observed under dark condition and is promoted by the appearance of light and the elevation of the intensity. Hence, a significant negative correlation exists between nitrate and nitrite products. Similar uneven promotion effect and negative dependence occur on authentic particles (Kaolin) as well. Based on the photo-electrochemical (PEC) tests and concentration dependence experiments, these illumination effects can be explained by the excess NO_2 adsorption under weak illumination while the sufficient photoinduced active species under strong irradiation.

The negative association between atmospheric nitrite and nitrate can be found in the presence of sunlight, along with the positive correlation in the absence of sunlight. The negative dependence can be explained by either the photolysis of particulate nitrate or the photoinduced oxidation of nitrite, suggesting illumination an inducing factor in the atmospheric nitrogen cycling. Nitrate pollution has got much concern recently, while little attention has been paid to the high nitrite concentrations accompanied by low nitrate levels. Nitrite may induce adverse health risk for its close association with various cancer cases **(Zhang et al., 2018)**. Compared to the nitrate-rich aerosols under strong irradiation, the nitrite-rich aerosols under faint sunlight may be more harmful to human health.

Actually, we discussed the γ-values based on the averaged experimental results while gave little care to various measurement errors. Compared to the arithmetic mean results, the percentile γ-values estimated by Monte Carlo simulation could be more suitable for modelling studies due to the differences between real atmosphere and the simulated laboratory condition. Furthermore, sensitivity analysis is helpful in explaining the determining factors involved in the assessment of uptake capacity. Generally, statistical simulation brings about more accurate evaluation and provides opportunities to explain the model discrepancy for secondary aerosols.

Data availability. All data are available upon request from the corresponding authors.

Supporting information. Sections on particle characterization, experimental setup, pretreatment for *in-situ* DRIFTS test, *ex-situ* flow reactor, uptake coefficient estimation, field observations, product observations, detailed reactions in photocatalytic process, photoinduced nitrite oxidation, Raman detection, Sensitivity analysis.

Author contributions. TW designed the experiments and wrote the paper. YYL and YD contributed to the DRIFTS spectra analysis. YYL and XZF support the field observation. HYC, YQF, MT, and XD assisted the Raman measurements. YY, KJL, SA, AB, and IN performed the PEC tests. LWZ guided the data analysis and paper writing. HBF and JMC provided some experimental facilities. All authors were involved in the discussion.

Competing interests. The authors declare no competing financial interests.

Acknowledgements. The authors gratefully acknowledge financial support from Ministry of Science and Technology of the People's Republic of China (2016YFE0112200, 2016YFC0202700), Marie Skłodowska-Curie Actions (690958-MARSU-RISE-2015), and National Natural Science Foundation of China (21507011, 21677037).

References

Anenberg, S.C., Miller, J., Minjares, R., Du, L., Henze, D.K.: Impacts and mitigation of excess diesel-related NO_x emissions in 11 major vehicle markets, Nature, 545, 467-471, doi: 10.1038/nature22086, 2017.

Balajka, J., Hines, M.A., DeBenedetti, W.J.I., Komora, M., Pavelec, J., Schmid, M., Diebold, U.: High-affinity adsorption leads to molecularly ordered interfaces on TiO_2 in air and solution, Science, 361, 786-789, doi: 10.1126/science.aat6752, 2018.

Ballari, M.M., Hunger, M., Hüsken, G., Brouwers, H.J.H.: NO_x photocatalytic degradation employing concrete pavement containing titanium dioxide, Applied Catalysis B: Environmental, 95, 245-254, doi: 10.1016/j.apcatb.2010.01.002, 2010.

Ballari, M.M., Yu, Q.L., Brouwers, H.J.H.: Experimental study of the NO and NO_2 degradation by photocatalytically active concrete, Catal. Today, 161, 175-180, doi: 10.1016/j.cattod.2010.09.028, 2011.

Baltrusaitis, J., Schuttlefield, J., Jensen, J.H., Grassian, V.H.: FTIR spectroscopy combined with quantum chemical calculations to investigate adsorbed nitrate on aluminium oxide surfaces in the presence and absence of co-adsorbed water, Phys. Chem. Chem. Phys., 9, 4970-4980, doi: 10.1039/b705189a, 2007.

Benedict, K.B., McFall, A.S., Anastasio, C.: Quantum Yield of Nitrite from the Photolysis of Aqueous Nitrate above 300 nm, Environ. Sci. Technol., 51, 4387-4395, doi: 10.1021/acs.est.6b06370, 2017.

Chen, H., Nanayakkara, C.E., Grassian, V.H.: Titanium dioxide photocatalysis in atmospheric chemistry, Chem. Rev., 112, 5919-5948, doi: 10.1021/cr3002092, 2012.

Chiang, K., Chio, C., Chiang, Y., Liao, C.: Assessing hazardous risks of human exposure to temple airborne polycyclic aromatic hydrocarbons, J. Hazard. Mater., 166, 676-685, doi: org/10.1016/j.jhazmat.2008.11.084, 2009.

Du, C., Kong, L., Zhanzakova, A., Tong, S., Yang, X., Wang, L., Fu, H., Cheng, T., Chen, J., Zhang, S.: Impact of adsorbed nitrate on the heterogeneous conversion of SO_2 on α-Fe_2O_3 in the absence and presence of simulated solar irradiation, Sci. Total Environ., 649, 1393-1402, doi: 10.1016/j.scitotenv.2018.08.295, 2019.

Dupart, Y., Fine, L., D'Anna, B., George, C.: Heterogeneous uptake of NO_2 on Arizona Test Dust under UV-A irradiation: An aerosol flow tube study, Aeolian Res., 15, 45-51, doi: org/10.1016/j.aeolia.2013.10.001, 2014.

El Zein, A., Bedjanian, Y.: Interaction of NO_2 with TiO_2 surface under UV irradiation: measurements of the uptake coefficient, Atmos. Chem. Phys., 12, 1013-1020, doi: 10.5194/acp-12-1013-2012, 2012.

Fu, Y., Kuppe, C., Valev, V.K., Fu, H., Zhang, L., Chen, J.: Surface-Enhanced Raman Spectroscopy: A Facile and Rapid Method for the Chemical Component Study of Individual Atmospheric Aerosol, Environ. Sci. Technol., 51, 6260-6267, doi: 10.1021/acs.est.6b05910, 2017.

FUJISHIMA, A., HONDA, K.: Electrochemical Photolysis of Water at a Semiconductor Electrode, Nature, 238, 37-38, doi: org/10.1038/238037a0, 1972.

Ginsberg, G.L., Belleggia, G.: Use of Monte Carlo analysis in a risk-based prioritization of toxic constituents in

house dust, Environ. Int., 109, 101-113, doi: 10.1016/j.envint.2017.06.009, 2017.
Goldstein, S., Rabani, J.: Mechanism of Nitrite Formation by Nitrate Photolysis in Aqueous Solutions: The Role of Peroxynitrite, Nitrogen Dioxide, and Hydroxyl Radical, J. Am. Chem. Soc., 129, 10597-10601, doi: 10.1021/ja073609, 2007.
Goodman, A.L., Miller, T.M., Grassian, V.H.: Heterogeneous reactions of NO_2 on NaCl and Al_2O_3 particles, Journal of Vacuum Science & Technology A: Vacuum, Surfaces, and Films, 16, 2585-2590, doi: 10.1116/1.581386, 1998.
Guan, C., Li, X., Luo, Y., Huang, Z.: Heterogeneous Reaction of NO_2 on α-Al_2O_3 in the Dark and Simulated Sunlight, J. Phys. Chem. A, 118, 6999-7006, doi: 10.1021/jp503017k, 2014.
Guo, S., Hu, M., Zamora, M.L., Peng, J., Shang, D., Zheng, J., Du, Z., Wu, Z., Shao, M., Zeng, L., Molina, M.J., Zhang, R.: Elucidating severe urban haze formation in China, Proceedings of the National Academy Sciences, 11, 17373-17378, doi: 10.1073/pnas.1419604111, 2014.
Gustafsson, R.J., Orlov, A., Griffiths, P.T., Cox, R.A., Lambert, R.M.: Reduction of NO_2 to nitrous acid on illuminated titanium dioxide aerosol surfaces: implications for photocatalysis and atmospheric chemistry, Chem. Commun., 0, 3936-3938, doi: 10.1039/B609005B, 2006.
Hems, R.F., Hsieh, J.S., Slodki, M.A., Zhou, S., Abbatt, J.P.D.: Suppression of OH Generation from the Photo-Fenton Reaction in the Presence of α-Pinene Secondary Organic Aerosol Material, Environmental Science & Technology Letters, 4, 439-443, doi: 10.1021/acs.estlett.7b00381, 2017.
Hou, X., Huang, X., Jia, F., Ai, Z., Zhao, J., Zhang, L.: Hydroxylamine Promoted Goethite Surface Fenton Degradation of Organic Pollutants., Environ. Sci. Technol., 51, 5118-5126, doi: 10.1021/acs.est.6b05906, 2017.
Huang, R.J., Zhang, Y., Bozzetti, C., Ho, K.F., Cao, J.J.: High secondary aerosol contribution to particulate pollution during haze events in China., Nature, 514, 218-222, doi: 10.1038/nature13774, 2014.
Kebede, M.A., Varner, M.E., Scharko, N.K., Gerber, R.B., Raff, J.D.: Photooxidation of Ammonia on TiO_2 as a Source of NO and NO_2 under Atmospheric Conditions, J. Am. Chem. Soc., 135, 8606-8615, doi: 10.1021/ja401846x, 2013.
Langridge, J.M., Gustafsson, R.J., Griffiths, P.T., Cox, R.A., Lambert, R.M., Jones, R.L.: Solar driven nitrous acid formation on building material surfaces containing titanium dioxide: A concern for air quality in urban areas? Atmos. Environ., 43, 5128-5131, doi: 10.1016/j.atmosenv.2009.06.046, 2009.
Li, H.J., Zhu, T., Zhao, D.F., Zhang, Z.F., Chen, Z.M.: Kinetics and mechanisms of heterogeneous reaction of NO_2 on $CaCO_3$ surfaces under dry and wet conditions, Atmos. Chem. Phys., 10, 463-474, doi: org/10.5194/acp-10-463-2010, 2010.
Li, J., Shang, J., Zhu, T.: Heterogeneous reactions of SO_2 on ZnO particle surfaces, Science China Chemistry, 54, 161-166, doi: org/10.1007/s11426-010-4167-9, 2010.
Liu, C., Ma, Q., Liu, Y., Ma, J., He, H.: Synergistic reaction between SO_2 and NO_2 on mineral oxides: a potential formation pathway of sulfate aerosol, Phys. Chem. Chem. Phys., 14, 1668-1676, doi: 10.1039/C1CP22217A, 2012.
Liu, Y., Han, C., Ma, J., Bao, X., He, H.: Influence of relative humidity on heterogeneous kinetics of NO_2 on kaolin and hematite, Phys. Chem. Chem. Phys., 17, 19424-19431, doi: 10.1039/C5CP02223A, 2015.
Ma, J., Liu, Y., He, H.: Heterogeneous reactions between NO_2 and anthracene adsorbed on SiO_2 and MgO, Atmos. Environ., 45, 917-924, doi: org/10.1016/j.atmosenv.2010.11.012, 2011.
Miller, T.M., Grassian, V.H.: Heterogeneous chemistry of NO_2 on mineral oxide particles: Spectroscopic evidence for oxide-coordinated and water-solvated surface nitrate, Geophys. Res. Lett., 25, 3835-3838, doi: org/10.1029/1998GL900011, 1998.
Monge, M.E., George, C., D Anna, B., Doussin, J., Jammoul, A., Wang, J., Eyglunent, G., Solignac, G., Daële, V., Mellouki, A.: Ozone Formation from Illuminated Titanium Dioxide Surfaces, J. Am. Chem. Soc., 132,

8234-8235, doi: 10.1021/ja1018755, 2010.
Moon, D.R., Taverna, G.S., Anduix-Canto, C., Ingham, T., Chipperfield, M.P., Seakins, P.W., Baeza-Romero, M., Heard, D.E.: Heterogeneous reaction of HO_2 with airborne TiO_2 particles and its implication for climate change mitigation strategies, Atmos. Chem. Phys., 18, 327-338, doi: 10.5194/acp-18-327-2018, 2018.
Moore, K.F., Eli Sherman, D., Reilly, J.E., Hannigan, M.P., Lee, T., Collett, J.L.: Drop size-dependent chemical composition of clouds and fogs. Part II: Relevance to interpreting the aerosol/trace gas/fog system, Atmos. Environ., 38, 1403-1415, doi: 10.1016/j.atmosenv.2003.12.014, 2004.
Nanayakkara, C.E., Larish, W.A., Grassian, V.H.: Titanium Dioxide Nanoparticle Surface Reactivity with Atmospheric Gases, CO_2, SO_2, and NO_2: Roles of Surface Hydroxyl Groups and Adsorbed Water in the Formation and Stability of Adsorbed Products, The Journal of Physical Chemistry C, 118, 23011-23021, doi: 10.1021/jp504402z, 2014.
Ndour, M., Anna, B.D., George, C., Ka, O., Balkanski, Y., Kleffmann, J., Stemmler, K., Ammann, M.: Photoenhanced uptake of NO_2 on mineral dust: Laboratory experiments and model simulations, Geophys. Res. Lett., 35, L5812, doi: org/10.1029/2007GL032006, 2008.
Niu, H., Li, K., Chu, B., Su, W., Li, J.: Heterogeneous Reactions between Toluene and NO_2 on Mineral Particles under Simulated Atmospheric Conditions, Environ. Sci. Technol., 51, 9596-9604, doi: 10.1021/acs.est.7b00194, 2017.
Ponczek, M., George, C.: Kinetics and product formation during the photooxidation of butanol on atmospheric mineral dust, Environ. Sci. Technol., 52, 5191-5198, doi:2018.
Schuttlefield, J., Rubasinghege, G., El-Maazawi, M., Bone, J., Grassian, V.H.: Photochemistry of Adsorbed Nitrate, J. Am. Chem. Soc., 130, 12210-12211, doi: 10.1021/jp902252s, 2008.
Shang, J., Li, J., Zhu, T.: Heterogeneous reaction of SO_2 on TiO_2 particles, Science China Chemistry, 53, 2637-2643, doi: org/10.1007/s11426-010-4160-3, 2010.
Su, H., Cheng, Y., Oswald, R., Behrendt, T., Trebs, I.: Soil nitrite as a source of atmospheric HONO and OH radicals., Science, 333, 1616-1618, doi: 10.1126/science.1207687, 2011.
Sun, Z., Kong, L., Ding, X., Du, C., Zhao, X., Chen, J., Fu, H., Yanga, X., Cheng, T.: The effects of acetaldehyde, glyoxal and acetic acid on the heterogeneous reaction of nitrogen dioxide on gamma-alumina, Phys. Chem. Chem. Phys., 18, 9367-9376, doi: 10.1039/C5CP05632B, 2016.
Syomin, D.A., Finlayson-Pitts, B.J.: HONO decomposition on borosilicate glass surfaces: implications for environmental chamber studies and field experiments, Phys. Chem. Chem. Phys., 5, 5236, doi: 10.1039/b309851f, 2003.
Szanyi, J., Kwak, J.H., Chimentao, R.J., Peden, C.H.F.: Effect of H_2O on the adsorption of NO_2 on γ-Al_2O_3: an in situ FTIR/MS study, The Journal of Physical Chemistry C, 111, 2661-2669, doi: 10.1021/jp066326x, 2007.
Szanyi, J., Kwak, J.H., Kim, D.H., Burton, S.D., Peden, C.H.F.: NO_2 Adsorption on BaO/Al_2O_3: The Nature of Nitrate Species, The Journal of Physical Chemistry B, 109, 27-29, doi: 10.1021/jp044993p, 2005.
Tan, F., Jing, B., Tong, S., Ge, M.: The effects of coexisting Na_2SO_4 on heterogeneous uptake of NO_2 on $CaCO_3$ particles at various RHs, Sci. Total Environ., 586, 930-938, doi: org/10.1016/j.scitotenv.2017.02.072, 2017.
Tan, F., Tong, S., Jing, B., Hou, S., Liu, Q., Li, K., Zhang, Y., Ge, M.: Heterogeneous reactions of NO_2 with $CaCO_3$-$(NH_4)_2SO_4$ mixtures at different relative humidities, Atmos. Chem. Phys., 16, 8081-8093, doi: 10.5194/acp-16-8081-2016, 2016.
Tang, M., Huang, X., Lu, K., Ge, M., Li, Y., Cheng, P., Zhu, T., Ding, A., Zhang, Y., Gligorovski, S., Song, W., Ding, X., Bi, X., Wang, X.: Heterogeneous reactions of mineral dust aerosol: implications for tropospheric oxidation capacity, Atmos. Chem. Phys., 17, 11727-11777, doi: 10.5194/acp-17-11727-2017, 2017.
Tang, S., Ma, L., Luo, M., Zhang, Z., Cao, X., Huang, Z., Xia, R., Qiu, Y., Feng, S., Zhang, P., Xia, C., Jin, Y., Xu, D.: Heterogeneous reaction of Cl_2 and NO_2 on γ-Al_2O_3: A potential formation pathway of secondary

aerosols, Atmos. Environ., 188, 25-33, doi: 10.1016/j.atmosenv.2018.06.005, 2018.
Underwood, G.M., Miller, T.M., Grassian, V.H.: Transmission FT-IR and Knudsen Cell Study of the Heterogeneous Reactivity of Gaseous Nitrogen Dioxide on Mineral Oxide Particles, The Journal of Physical Chemistry A, 103, 6184-6190, doi: 10.1021/jp991586i, 1999.
Usher, C.R., Michel, A.E., Grassian, V.H.: Reactions on mineral dust, Chem. Rev., 103, 4883-4940, doi: 10.1021/cr020657y, 2003.
Wang, L., Wang, W., Ge, M.: Heterogeneous uptake of NO_2 on soils under variable temperature and relative humidity conditions, J. Environ. Sci.-China, 24, 1759-1766, doi: org/10.1016/S1001-0742(11)61015-2, 2012.
Wang, L., Wen, L., Xu, C., Chen, J., Wang, X., Yang, L., Wang, W., Yang, X., Sui, X., Yao, L., Zhang, Q.: HONO and its potential source particulate nitrite at an urban site in North China during the cold season, Sci. Total Environ., 538, 93-101, doi: 10.1016/j.scitotenv.2015.08.032, 2015.
Wang, T., Liu, Y., Deng, Y., Fu, H., Zhang, L., Chen, J.: Adsorption of SO_2 on mineral dust particles influenced by atmospheric moisture, Atmos. Environ., 191, 153-161, doi: 10.1016/j.atmosenv.2018.08.008, 2018a.
Wang, T., Liu, Y., Deng, Y., Fu, H., Zhang, L., Chen, J.: The influence of temperature on the heterogeneous uptake of SO_2 on hematite particles, Sci. Total Environ., 644, 1493-1502, doi: 10.1016/j.scitotenv.2018.07.046, 2018b.
Wang, T., Liu, Y., Deng, Y., Fu, H., Zhang, L., Chen, J.: Emerging investigator series: heterogeneous reactions of sulfur dioxide on mineral dust nanoparticles: from single component to mixed components, Environmental Science: Nano, 5, 1821-1833, doi: 10.1039/C8EN00376A, 2018c.
Wu, L., Tong, S., Ge, M.: Heterogeneous Reaction of NO_2 on Al_2O_3: The Effect of Temperature on the Nitrite and Nitrate Formation, J. Phys. Chem. A, 117, 4937-4944, doi: 10.1021/jp402773c, 2013.
Xia, Z., Duan, X., Tao, S., Qiu, W., Liu, D., Wang, Y., Wei, S., Wang, B., Jiang, Q., Lu, B., Song, Y., Hu, X.: Pollution level, inhalation exposure and lung cancer risk of ambient atmospheric polycyclic aromatic hydrocarbons (PAHs) in Taiyuan, China, Environ. Pollut., 173, 150-156, doi: 10.1016/j.envpol.2012.10.009, 2013.
Xue, J., Yuan, Z., Griffith, S.M., Yu, X., Lau, A.K.H., Yu, J.Z.: Sulfate Formation Enhanced by a Cocktail of High NO_x, SO_2, Particulate Matter, and Droplet pH during Haze-Fog Events in Megacities in China: An Observation-Based Modeling Investigation, Environ. Sci. Technol., 50, 7325-7334, doi: 10.1021/acs.est.6b00768, 2016.
Yang, W., Chen, M., Xiao, W., Guo, Y., Ding, J., Zhang, L., He, H.: Molecular Insights into NO-Promoted Sulfate Formation on Model TiO_2 Nanoparticles with Different Exposed Facets, Environ. Sci. Technol., 52, 14110-14118, doi: 10.1021/acs.est.8b02688, 2018.
Yang, Y., Teng, F., Kan, Y., Yang, L., Liu, Z., Gu, W., Zhang, A., Hao, W., Teng, Y.: Investigation of the charges separation and transfer behavior of BiOCl/BiF_3 heterojunction, Applied Catalysis B: Environmental, 205, 412-420, doi: 10.1016/j.apcatb.2016.12.062, 2017.
Ye, C., Gao, H., Zhang, N., Zhou, X.: Photolysis of Nitric Acid and Nitrate on Natural and Artificial Surfaces, Environ. Sci. Technol., 50, 3530-3536, doi: 10.1021/acs.est.5b05032, 2016.
Ye, C., Zhang, N., Gao, H., Zhou, X.: Photolysis of Particulate Nitrate as a Source of HONO and NO_x, Environ. Sci. Technol., 51, 6849-6856, doi: 10.1021/acs.est.7b00387, 2017.
Yi, C., Kwak, J.H., Peden, C.H.F., Wang, C., Szanyi, J.: Understanding Practical Catalysts Using a Surface Science Approach: The Importance of Strong Interaction between BaO and Al_2O_3 in NO_x Storage Materials, The Journal of Physical Chemistry C, 111, 14942-14944, doi: 10.1021/jp0763376, 2007.
Yu, T., Zhao, D., Song, X., Zhu, T.: NO_2-initiated multiphase oxidation of SO_2 by O_2 on $CaCO_3$ particles, Atmos. Chem. Phys., 18, 6679-6689, doi: 10.5194/acp-2017-900, 2018.
Yu, Z., Jang, M.: Simulation of heterogeneous photooxidation of SO_2 and NO_2; in the presence of Gobi Desert

dust particles under ambient sunlight, Atmos. Chem. Phys., 18, 14609-14622, doi: 10.5194/acp-2018-68, 2018.
Zhang, P., Lee, J., Kang, G., Li, Y., Yang, D., Pang, B., Zhang, Y.: Disparity of nitrate and nitrite in vivo in cancer villages as compared to other areas in Huai River Basin, China, Sci. Total Environ., 612, 966-974, doi: 10.1016/j.scitotenv.2017.08.245, 2018.
Zhang, R., Wang, G., Guo, S., Zamora, M.L., Ying, Q., Lin, Y., Wang, W., Hu, M., Wang, Y.: Formation of Urban Fine Particulate Matter, Chem. Rev., 115, 3803-3855, doi: 10.1021/acs.chemrev.5b00067, 2015.
Zhang, Z., Shang, J., Zhu, T., Li, H., Zhao, D., Liu, Y., Ye, C.: Heterogeneous reaction of NO_2 on the surface of montmorillonite particles, J. Environ. Sci.-China, 24, 1753-1758, doi: org/10.1016/S1001-0742(11)61014-0, 2012.
Zhao, D., Song, X., Zhu, T., Zhang, Z., Liu, Y.: Multiphase oxidation of SO_2 by NO_2 on $CaCO_3$ particles, Atmos. Chem. Phys., 18, 2481-2493, doi: 10.5194/acp-2017-610, 2018.
Zheng, X., Li, D., Li, X., Chen, J., Cao, C., Fang, J., Wang, J., He, Y., Zheng, Y.: Construction of ZnO/TiO_2 photonic crystal heterostructures for enhanced photocatalytic properties, Applied Catalysis B: Environmental, 168-169, 408-415, doi: 10.1016/j.apcatb.2015.01.001, 2015.